Displays 54 (2018) 1–8

Contents lists available at ScienceDirect

Displays

journal homepage: www.elsevier.com/locate/displa

Perceptual brightness-based inverse tone mapping for high dynamic range imaging☆

Gwon Hwan An, Yong Deok Ahn, Siyeong Lee, Suk-Ju Kang*

Department of Electronic Engineering, Sogang University, Seoul 04107, Republic of Korea

ARTICLE INFO

Keywords:
High dynamic range
Inverse tone mapping
Tone mapping

ABSTRACT

This paper proposes a novel high dynamic range imaging method based on inverse tone mapping for generating a high dynamic range image from a single low dynamic range image. With the increasing expectations for image quality, displays providing high dynamic range images have been released. However, although low dynamic range images are currently commonly used, they do not use the high representation capability of high dynamic range displays. Moreover, high dynamic range contents are scarce. Therefore, high dynamic range imaging techniques are gaining attention. The proposed method involves adaptive specular region detection to determine the bright and dark areas for high dynamic range imaging, output mapping range decision to consider perceptual brightness, final mapping-level decision to prevent degradation of perceptual image quality, and inverse pixel mapping for luminance mapping. The simulation results of the proposed method yielded an HDR-VDP-2 quality score of 59.51, which was higher than those of the conventional methods. Furthermore, the execution time of the proposed algorithm was 0.66 s, which had the lowest complexity compared to the conventional methods. For subjective performance evaluation, we analyzed the perceived image quality on the display with the DRIM, which confirmed the superiority of the proposed method over the conventional methods.

1. Introduction

With the increased expectation for image quality, a display system capable of significantly enhancing the perceived image quality by increasing the color reproduction has gained attention. Furthermore, because of the increase in the maximum emitting luminance and color gamut of the display, the high dynamic range (HDR) imaging in the display has been prevalent [1–4]. Typically, in a conventional display system, the number of bits per pixel is 8, which has been increased to 10 bits or more in recent years to display a high-luminance image. Currently, technologically applicable displays output over 1000 nit for a liquid crystal display (LCD) and over 700 nit for an organic light emitting diode display (OLED). Using HDR displays requires HDR contents; however, insufficient contents and broadcasting equipment make it challenging to effectively use the HDR display.

Therefore, HDR imaging has been studied; however, improving the performance and reducing complexity are still essential. We propose a novel HDR imaging method that can be applied to real-time applications for improving performance. The proposed method involves adaptive specular region detection to determine the bright and dark areas for HDR imaging, output mapping range decision to consider perceptual brightness, final mapping-level decision to prevent degradation of perceptual image quality, and inverse pixel mapping for luminance mapping.

This paper is organized as follows. Section 2 introduces the concept of the existing HDR imaging techniques. We introduce two methods, namely, using multiple-exposure images and a single-exposure image, and analyze the advantages and disadvantages of each method. In addition, a method for detecting various specular areas required for HDR imaging is discussed. Section 3 elucidates the procedure for performing the proposed HDR imaging using a single image. In Section 4, we introduce the simulation environments and results obtained by comparing the proposed and conventional methods. Finally, in Section 5, we conclude the paper.

2. Related works

As a representative method of HDR imaging, there are methods for HDR image gradation mapping using multiple- and single-exposure images. Debevec et al. [5] proposed a method to recover HDR radiance map from multiple-exposure images. For multiple-exposure images generated with varying aperture and shutter speed of a camera, the

☆ This paper was recommended for publication by Pen-Cheng Wang.

* Corresponding author.
E-mail address: sjkang@sogang.ac.kr (S.-J. Kang).

https://doi.org/10.1016/j.displa.2018.07.003
Received 14 May 2018; Accepted 11 July 2018
Available online 17 July 2018

details of gradation in the dark and bright areas differ depending on the exposure level. HDR imaging can be performed using the characteristic that the gradation detail of the bright and dark areas is preserved with low exposure and high exposure, respectively. However, in this method, acquiring multiple-exposure images and applying in a real-time application is challenging. Therefore, we propose the HDR imaging method using a single-exposure image. Rempel et al. [6] proposed an inverse tone mapping (ITM) for HDR imaging, using LDR information of the single-exposure image. This method divides the bright and dark regions according to the brightness level of each region. Specifically, they used a fixed threshold value to determine the bright region, and then used the Gaussian function with considering the maximum display luminance for generating the brightness enhancement function. Furthermore, they used the edge-stopping function that considers the large brightness difference in the surrounding region to accurately detect the bright region. However, due to fixed threshold value and edge stopping, the detection performance is not robust, according to the image characteristics. Moreover, because the range of an input image for the HDR display was linearly stretched, the output luminance of very high display resulted in unnatural images. Meylan et al. [7] proposed an ITM method that extracted specular areas, divided the image into specular and diffuse areas, subdivided the brightness gradations of the specular areas, and adjusted the brightness gradation of the diffuse areas. This method reproduces the specular region, thereby solving the problem that, when the conventional LDR image is directly outputted to the HDR display, the overall brightness of the image is increased. The specular region is a portion where light reflects by direct rays and saturates when the information is stored in the camera, thereby causing loss of detailed information. Increasing the slope of the curve to map the brightness gradation of the specular region and lowering the slope of the diffuse area to lower the overall brightness gradation generates an image with larger dynamic range in the searched specular area, as well as hardware implementation issues can be considered. However, the specular reproduction method had several problems in HDR imaging. First, when extracting the specular region from an input image, the performance varied according to the size of the specular region and kernel size of the filter because the threshold is derived by using two low-pass filters having different kernel sizes. In addition, changing the threshold of the specular region according to the input image, failed to assure the final performance of the HDR imaging, because the output mapping level was fixed, and hence, the perceptual brightness was not considered. Second, they attempted to solve the problem that occurs when mapping the brightness gradation by abruptly breaking the curve of the specular area using contour smoothing. However, due to the lack of detection performance and details deterioration of the specular area, the perceived quality of the output HDR image was poor. Huo et al. [8] proposed an HDR imaging method that reflected the local retina response, unlike the area-based methods [6,7]. In this method, the HDR brightness was calculated by simultaneously considering the brightness information of the input image, local average brightness, and local retina response. As bilateral filtering was used to calculate the local average brightness, the local average brightness was extracted by reducing the noise while preserving the edge. In addition, a good perceptual image quality was derived because the HDR image was generated by simultaneously considering the human visual model. However, the calculation of the local average brightness of the LDR image and mapping of the HDR image using the sigmoid curve for the local adaptive response degraded the gradation refinement of the saturated region. Furthermore, recursively performing bilateral filtering for considering the local average brightness to find the optimal value made it difficult to apply real-time application than other methods. Masia et al. [9] proposed a method of performing gamma expansion based on HDR imaging using image statistics. They obtained the optimal gamma curve by considering that the saturated region is different for different exposures of a single image. This method eliminated gamma correction of the image by performing gamma decoding and proceeded with the camera data-based analysis. For the low- and high-exposure images, because the dark and bright regions, respectively, are saturated, the gradation was refined by the HDR expansion with a low- and high-value gamma curve, respectively. Thus, the saturated area in each image was mapped into the HDR image by finding the appropriate gamma curve to fine-tune the gradation of the area. However, because mapping was determined by the gamma curve after the image analysis, the gradation refinement of the saturated region was difficult. Moreover, each mapping section did not consider the display output luminance, a perceptual image quality degradation may occur.

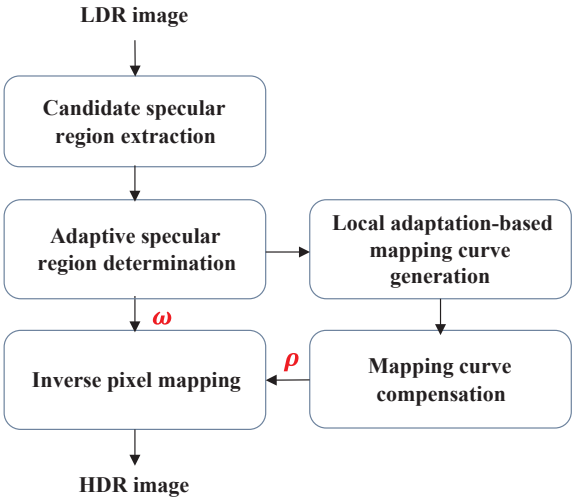

Fig. 1. Overall flowchart of the proposed PB-ITM-based HDR imaging.

3. Proposed method

The proposed perceptual brightness-based ITM (PB-ITM) for HDR imaging generates HDR images using a single LDR image as shown in Fig. 1. It analyzes an input LDR image and searches for a candidate specular region having a high probability to be a specular region. We detect the specular region using the average specular reflectance of the image. Furthermore, we calculate the brightness of the specular region using the local adaptation based on the retina response for determining the optimal output mapping range. In addition, we determine the final mapping level by using the weber contrast to prevent degradation of the perceptual image quality. Finally, we perform PB-ITM using the determined threshold and final mapping curve.

3.1. Candidate specular region extraction

First, we detect candidate specular regions with the high possibility to be a specular region. Before detecting the area, gamma decoding is performed:

$$I_R = (I'_R)^\gamma, \quad I_G = (I'_G)^\gamma \quad I_B = (I'_B)^\gamma, \tag{1}$$

where I'_R, I'_G, and I'_B are the R, G, and B channels of a gamma corrected image, respectively. γ is a gamma value, and I_R, I_G, and I_B are R,

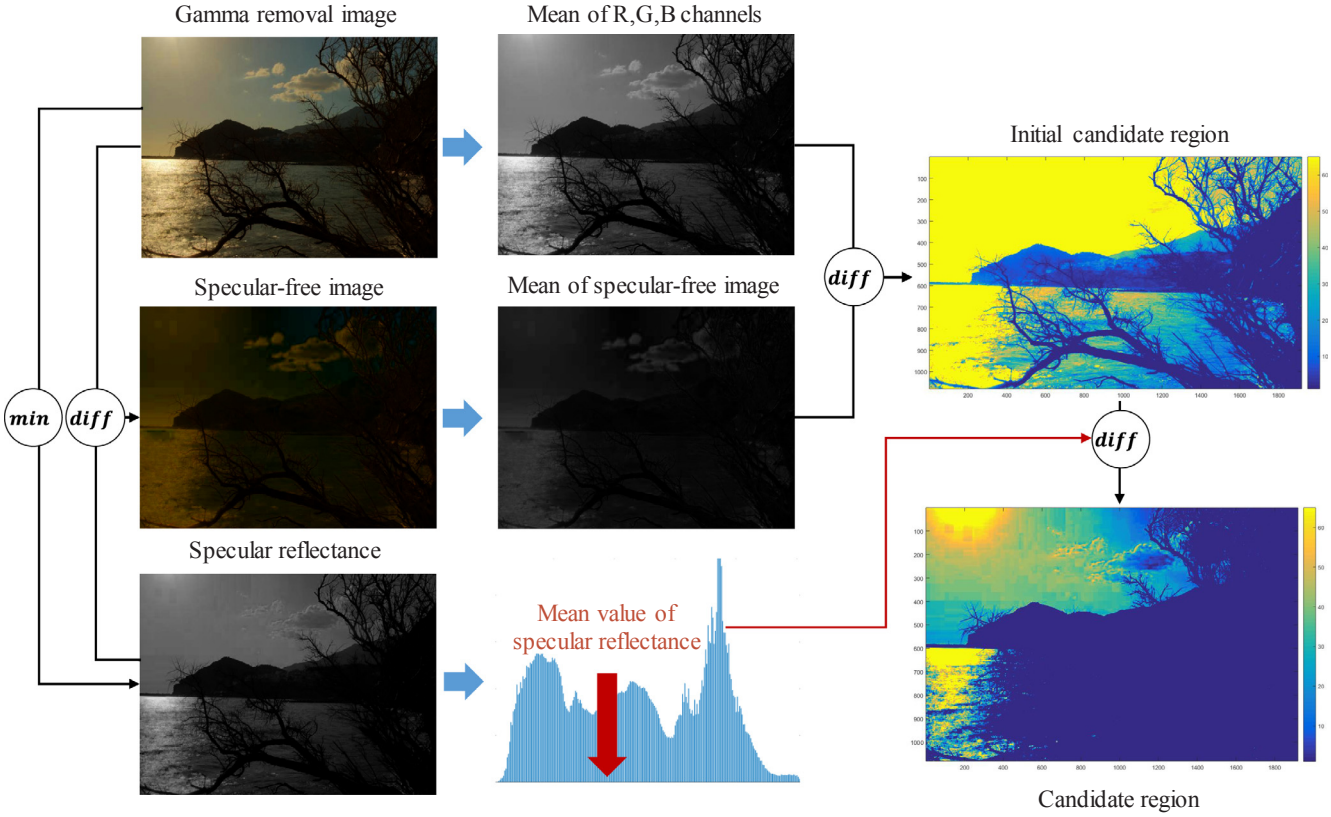

Fig. 2. Candidate specular region extraction in the proposed method, including gamma decoding and initial candidate region detection.

G, and B channels, respectively, after applying gamma decoding.

Fig. 2 outlines the proposed candidate specular region detection. First, we define specular reflectance of the minimum value of RGB data using the specular-free method proposed by Shen et al. [10], which generates RGB data of the specular-free image. Eq. (2) defines the specular reflectance and the specular-free image:

$$\begin{aligned} S_r &= min\{I_R, I_G, I_B\}, \\ I_{sf\_RGB} &= [I_R - S_r, I_G - S_r, I_B - S_r], \end{aligned} \tag{2}$$

where S_r is a specular reflectance component and I_{sf_RGB} denotes a specular-free image.

Then, using Eq. (3), we obtain the RGB data average of the gamma-decoded input image, specular-free image, and specular reflectance:

$$\begin{aligned} I_{avg} &= \tfrac{1}{3}(I_R + I_G + I_B), \\ I_{sf\_avg} &= \tfrac{1}{3}(I_{sf\_R} + I_{sf\_G} + I_{sf\_B}), \\ \overline{S}_r &= \tfrac{1}{N}\textstyle\sum_{x=1}^{N} S_r(x), \end{aligned} \tag{3}$$

where I_{avg} and I_{sf_avg} denote the average for RGB channels of the gamma-decoded input image and the specular-free image, respectively, N is the total number of pixels, and S_r is the average of the specular reflectance.

We detect the initial candidate specular region by subtracting the RGB data average of the specular-free image from the RGB data average of the gamma-decoded input image. Subtracting the mean value of the specular reflectance from the initial candidate specular region causes the diffuse region to disappear. We extract only the region beyond the mean value of the specular reflectance. Eq. (4) defines this region as the candidate specular region:

$$SH_{cand} = I_{avg} - I_{sf\_avg} - \overline{S}_r \tag{4}$$

where SH_{cand} is the candidate specular region.

3.2. Adaptive specular region determination

We use adaptive thresholding for detecting the final specular region in candidate specular regions. Fig. 3(a) shows that, after generating the histogram of the candidate specular region, if the average of the specular reflectance $\overline{S}_r$ is low, the specular region is decreased by setting the threshold higher. Otherwise, the specular region is increased by setting the threshold lower. Eq. (5) defines the adaptive threshold TH:

$$TH = \begin{cases} min(X), where\ C(X) > S_{th},\ X = 1, \cdots, M \\ M, \qquad otherwise \end{cases} \tag{5}$$

where

$$\begin{aligned} S_{th} &= \tfrac{C(M)}{M}(max\{S_r\} - \overline{S}_r), \\ C(M) &= |\{i | H(i) > 0,\ i = 1, \ldots, M\}|, \end{aligned}$$

H is the histogram of a candidate specular region, M is the total number of representative values, and $C(M)$ is the number of representative values, which are non-zero. S_{th} is a parameter based on the reflectance component, and TH is the threshold that determines the specular region.

After extracting the specular region above the threshold, we transform the specular region and the threshold from the brightness domain

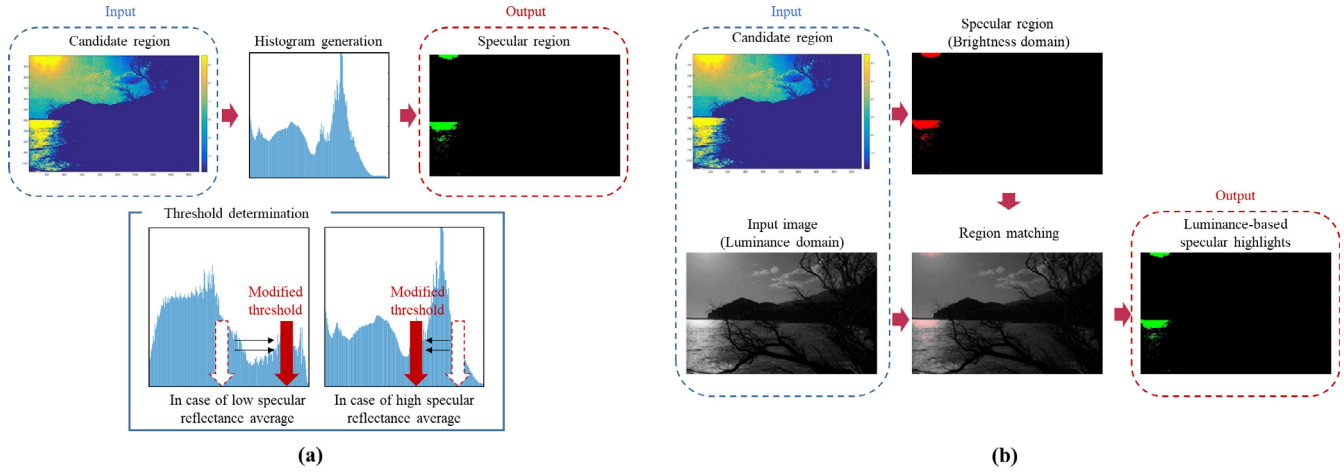

Fig. 3. Determination of luminance-based specular highlights: (a) adaptive specular region determination and (b) region matching for transformation from the brightness domain to the luminance domain.

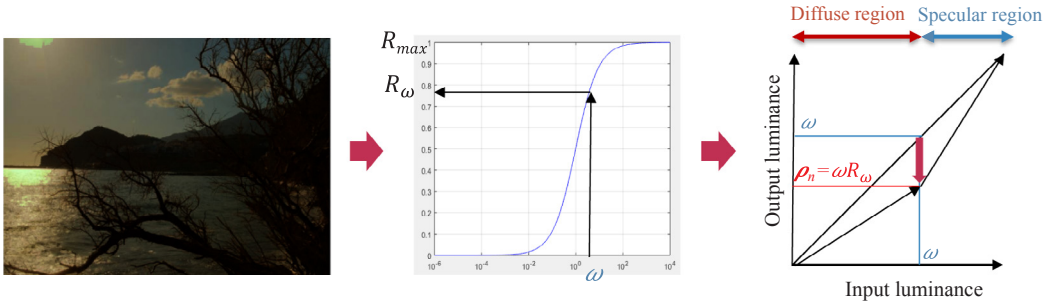

Fig. 4. Output mapping range change using the perception brightness calculation when the diffuse region is the background in the local area.

to the luminance domain, for considering the retina response. As shown in Fig. 3(b), we perform region matching between the brightness domain and luminance domain to acquire the luminance level of the detected specular region. Then, we extract the luminance-based specular highlights.

3.3. Local adaptation based mapping curve generation

After determining the luminance-based threshold ω from the brightness-based threshold TH, we decide the output mapping level. To determine the range of output mapping levels, we use the local adaptation-based retina response model to consider the human perception, which is defined in Eq. (6).

$$R = R_{max}\frac{L^n}{L^n + \sigma^n} \tag{6}$$

where R is the retina response, R_{max} is the maximum value of the response, L is the light intensity, σ is an adaptation level, and n is a coefficient that determines the curve sensitivity of the retina response.

Specifically, using the local adaptation level-based retina response model, we consider the human-perceived luminance level in the local area [11–13]. The response is defined using the characteristic that the perceived brightness changes when the background brightness changes in the local area.

Fig. 4 illustrates the perception of the specular region by humans, using the local adaptive retina response, and determines the output mapping range based on this result. Eq. (7) denotes the method for determining the output mapping range:

$$\rho_n = \omega R_\omega \tag{7}$$

where

$$R_\omega = R_{max}\frac{\omega^n}{\omega^n + D_{apl}^n},$$

$$D_{apl} = \frac{1}{N}\sum_{\{x|I_Y(x) < \omega\}} I_Y(x),$$

I_Y is the luminance value of the input image, ω is the luminance-based specular threshold, N is the pixel number of diffuse region, D_{apl} is the average luminance of the diffuse region, R_ω is the value of the region-based retina response, and ρ_n is the value of an output mapping breakpoint, as shown in Fig. 4.

After computing the average luminance level of the diffuse region, we calculate the local adaptation level based on the retina response to calculate the perceived brightness. For a darker perceived specular region, we widen the output mapping range of the specular region, thereby lowering the minimum mapping level and the overall luminance gradation of the diffuse region. Therefore, we subdivide the luminance gradation of the specular region while making the specular region perceptually brighter. Then, we determine the breakpoint of the final mapping curve by using the weber contrast after determining the output mapping range based on the image information and perceptual characteristics.

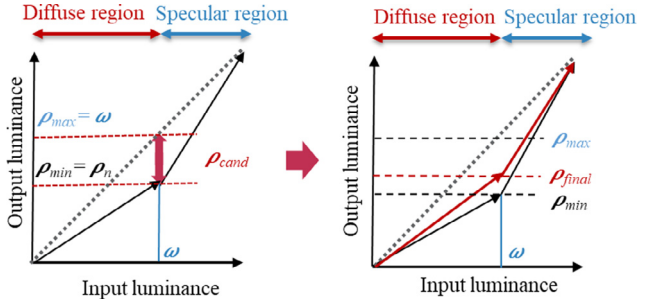

Fig. 5. Final mapping curve decision in the candidate output luminance level range ($\rho_{min} \sim \rho_{max}$).

3.4. Mapping curve compensation

With the breakpoint of the final mapping curve at the mapping level ρ_n considering only the local adaptation level, the range of the specular region is very wide in some images. This may degrade the diffuse region, thereby degrading the perceived image quality. To prevent this, we constrain the range of the breakpoint to the maximum value as ω and the minimum value as ρ_n, and we consider the perceptual contrast ratio of the local region based on the output luminance and the weber contrast of the display device. Eq. (8) defines the minimum and maximum values of the mapping range and the candidate mapping level. Fig. 5 illustrates the concept of candidate mapping level and the breakpoint of the final mapping curve in the ITM-based HDR imaging.

$$\rho_{cand} = (1-\beta)\rho_{min} + \beta\rho_{max} (0 \le \beta \le 1) \tag{8}$$

where

$$\rho_{max} = \omega,$$
$$\rho_{min} = \rho_n,$$

ρ_{max} and ρ_{min} are the maximum and minimum mapping level, respectively, and ρ_{cand} is the candidate level using the weighted average.

We determine the candidate mapping level between the maximum and minimum mapping levels. We use the weber contrast-based equation to determine the final breakpoint using the candidate mapping level, as in Eq. (9):

$$SH_{wc} = \frac{S_{apl} - \rho_{cand}}{\rho_{cand}},$$
$$DF_{wc} = \frac{D_{apl} - \rho_{cand}}{\rho_{cand}}, \tag{9}$$

where S_{apl} is the average luminance of the specular region, SH_{wc} and DF_{wc} are the weber contrasts of the specular and diffuse region, respectively.

Then, we change the candidate mapping level until finding the point where the weber contrast of the specular and diffuse regions is equal. We determine the point as the breakpoint of the final mapping curve, as in Eq. (10), which is changed as Eq. (11). We derive Eq. (12) from Eq. (11). Because the average luminance value of the specular region is not equal to the average luminance value of the diffuse region, we can derive Eq. (13) from Eq. (12). By considering Eqs. (13), (14) defines the breakpoint of the final mapping curve:

$$\rho_{final} = \rho_{cand} \ if \ |SH_{wc}| = |DF_{wc}| \tag{10}$$

$$|SH_{wc}| = |DF_{wc}|,$$
$$\left|\frac{S_{apl} - \rho_{cand}}{\rho_{cand}}\right| = \left|\frac{D_{apl} - \rho_{cand}}{\rho_{cand}}\right|, \tag{11}$$

$$|S_{apl} - \rho_{cand}|^2 = |D_{apl} - \rho_{cand}|^2,$$
$$S_{apl}^2 - 2S_{apl}\rho_{cand} + 2D_{apl}\rho_{cand} - D_{apl}^2 = 0,$$
$$(S_{apl} - D_{apl})(S_{apl} + D_{apl}) - 2\rho_{cand}(S_{apl} - D_{apl}) = 0,$$
$$(S_{apl} - D_{apl})(S_{apl} + D_{apl} - 2\rho_{cand}) = 0, \tag{12}$$

$$(S_{apl} + D_{apl}) = 2\rho_{cand} \tag{13}$$

$$\rho_{final} = \rho_{cand} = \frac{(S_{apl} + D_{apl})}{2} \tag{14}$$

where ρ_{final} is the breakpoint of the final mapping curve where the weber contrast of the specular and diffuse regions is same.

3.5. Inverse pixel mapping

For generating the final HDR image, we use the previously determined luminance-based specular threshold and final mapping level. We refine the gradation of the diffuse region by using the average luminance to transform the curve, as shown in Fig. 6(a). When generating the HDR image by the proposed method, the gradation of the whole image can be refined by considering the perceptual brightness of the specular area. For applying inverse pixel mapping, we define each slope in Fig. 6(b) as in Eq. (15). The proposed method performs inverse pixel mapping as follows:

$$I_{TM}(x) = \begin{cases} s_1 I_Y(x), & if \ I_Y(x) < D_{apl} \\ s_2 (I_Y(x) - D_{apl}) + s_1 D_{apl}, & if \ D_{apl} < I_Y(x) \le \omega \\ s_3 (I_Y(x) - max\{I_Y\}) + max\{d_Y\}, & if \ I_Y(x) > \omega \end{cases} \tag{15}$$

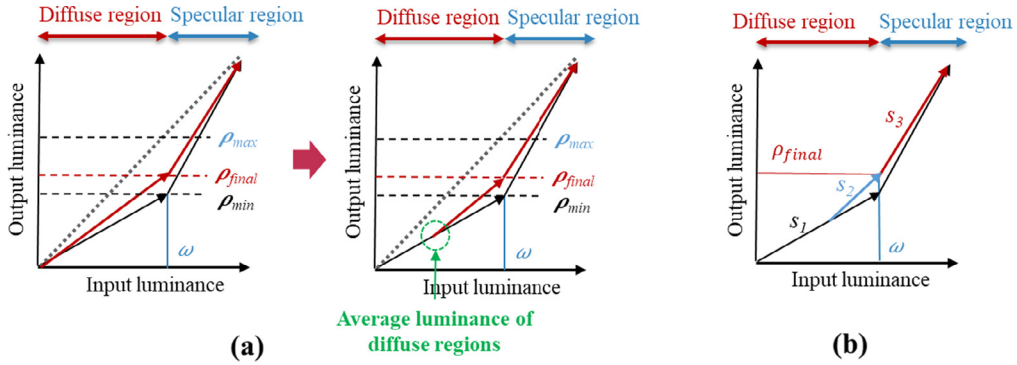

Fig. 6. Proposed inverse pixel mapping curve: (a) the average luminance of the diffuse region is considered to refine the gradation of the diffuse region and (b) final inverse pixel mapping curve decision ($s_1 \sim s_2 \sim s_3$).

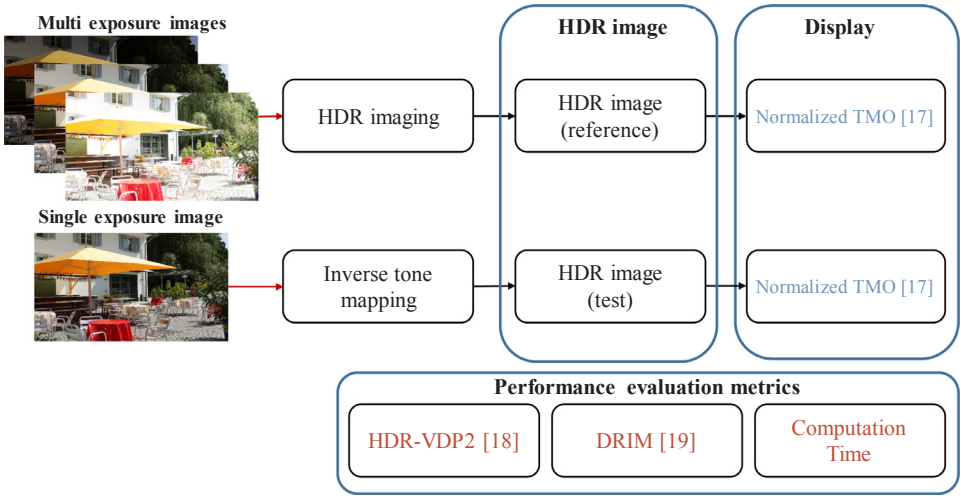

Fig. 7. Evaluation environment for evaluating the performance of the proposed and conventional methods.

where

$$s_1 = \frac{\rho}{\omega},$$

$$s_2 = \frac{\rho_{final} - D_{apl} s_1}{\omega - D_{apl}},$$

$$s_3 = \frac{\max\{d_Y\} - \rho_{final}}{\max\{\mathrm{I_Y}\} - \omega}.$$

s_1, s_2, and s_3 are slopes in each region for PB-ITM-based HDR imaging of Fig. 5(b), and d_Y is the display output luminance.

4. Simulation results

Fig. 7 shows the evaluation environment for performance comparison of the proposed method. In the dataset for the simulation, we used the datasets obtained by multiple exposures by varying the camera exposure for the simulation [14–16]. We used 128 image stacks for comparing the HDR toolbox [17]. We selected the LDR image with the most even histogram distribution among multiple exposure images as an input because we assumed that existing LDR images are generally well-exposed that represent a detailed image. We compared the proposed method with that of Debevec et al. [5] as a ground truth and the existing ITM methods [7–9] by generating the HDR image. For the evaluation metric, we used the HDR visual difference predictor 2 (HDR-VDP-2) [18] and dynamic range-independent image quality assessment (DRIM) [19], the most popular evaluation metrics. HDR-VDP-2 is an HDR evaluation method that uses the detection map and the VDP-quality score that can derive the probability of the difference between the two images at which a typical observer can recognize. In the detection map, a low probability of noticing the difference between the two images generates a blue pixel; otherwise, a red pixel. In addition, the VDP-quality score determines the image quality by measuring the loss of the test image relative to the reference image. DRIM is illustrates the difference between HDR images. In the DRIM, red, green, and blue points indicate the contrast reversal, loss of visible contrast, and amplification of invisible contrast relative to the reference image, respectively. Furthermore, as a benchmark for the performance evaluation of PB-ITM, we compared the computational generation time of each method. The computational generation time is measured with a PC with an Intel i5-6500 3.20 GHz CPU. Moreover, we described the generated HDR images using the normalized tone mapping operator (TMO) [17] for visualization.

Fig. 8 shows the results of TMO, the probability of detection map, VDP-quality score, and DRIM with the ground truth HDR images using the multiple-exposure-based method [5]. As shown in Fig. 8(a), the area-based method [7] had high error probability in the specular region because the specular detection performance of [7] was relatively poor. The sigmoid-based mapping curve method [8] had high error probability in the saturated region because a sigmoid-based mapping curve degrades the gradation of the saturated region. The gamma expansion method based on image statistics [9] had many areas where high error probability was observed due to not considering the region information. In the proposed method, the high error probability area was relatively small due to considering the perceptual brightness of the specular area and the uniformity of the curve based on the weber contrast. Furthermore, DRIM results show that the proposed method had less number of green points at the boundary of specular region, indicating that it expanded the input range more naturally by using the local adaptation. Fig. 8(b) and (c) show the results when the input image was bright overall. In this case, the mapping curve slope of the specular region in the proposed method deflected to increase the relative luminance of the specular region. Therefore, the probability of difference detection in the bright region was decreased, thereby generating an output high-quality image. DRIM results indicate that the proposed method had the lowest number of green points than other methods. Table 1 presents objective comparisons of the average VDP-quality score and computational generation time. In the case of the VDP-quality score, the proposed method was the highest (59.5068) and [8] was the lowest (57.7971). For the HDR image generation time, the proposed method was the fastest (0.6599 s), indicating low computational complexity and the method of [8] was the lowest (1.410 s). Therefore, we confirm that the proposed method performed best than other conventional methods.

5. Conclusion

In this paper, we proposed the PB-ITM-based HDR imaging to generate an HDR image only using a single LDR image to solve the problem of displaying the LDR image to the HDR display. The proposed method improved the gradation expression of specular and diffuse areas

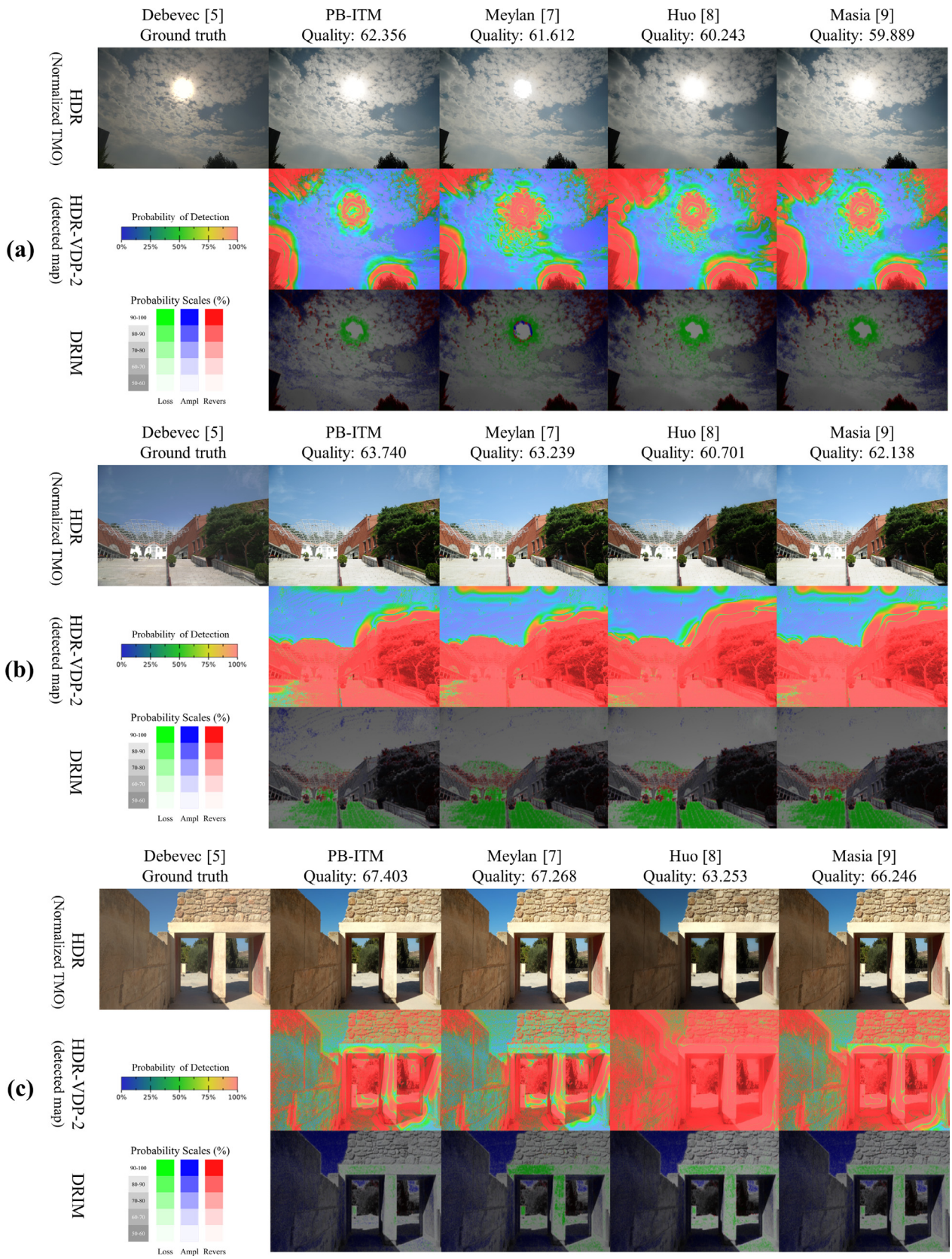

Fig. 8. Comparison results of TMO, the probability of detection map, VDP-quality score, and DRIM with the ground truth HDR images using multiple-exposure-based method in the case of large specular region (a), in the case of bright images (b), (c).

Table 1
Comparison of the VDP-quality score and computation time of conventional and proposed methods.

Type of Image	VDP-quality score		Computation time [s]	
	Avg.	Std.	Avg.	Std.
Meylan et al. [7]	58.8782	4.9924	1.2153	0.0328
Huo et al. [8]	57.7971	4.7201	1.4100	0.0472
Masia et al. [9]	58.9069	5.3367	0.9955	0.0460
Proposed PB-ITM	59.5068	5.4077	0.6599	0.0356

by adaptive specular area detection using specular reflectance, output mapping range determination using local adaptation, and final mapping-level determination based on the weber contrast. In the experimental results, the HDR-VDP-2 quality score of the proposed method was 59.5068, which was higher than those of the existing methods. Furthermore, we confirmed that the qualitative image quality was superior to that of other methods, and the algorithm computation was the lowest (0.6599 s). By considering both quantitative and qualitative performance evaluation, we confirm that the proposed PB-ITM has the best performance.

Conflict of interest

The authors declared that there is no conflict of interest.

Acknowledgement

This research was supported by the MSIT(Ministry of Science and ICT), Korea, under the ITRC(Information Technology Research Center) support program(IITP-2018-0-01421) supervised by the IITP(Institute for Information & communications Technology Promotion) and the Korea Institute of Energy Technology Evaluation and Planning(KETEP) and the Ministry of Trade, Industry & Energy(MOTIE) of the Republic of Korea (No. 20161210200560).

References

[1] ITU-R Recommendation BT.2020: parameter values for ultra-high definition television systems for production and international program exchange, Int. Telecommun. Union, 2012.
[2] ST 2084:2014 – SMPTE Standard – High dynamic range electro-optical transfer function of mastering reference displays, SMPTE ST 20842014, 2014, 1–14.
[3] ST 2086:2014 – SMPTE Standard – Mastering display color volume metadata supporting high luminance and wide color gamut images, ST 20862014, 2014 1–6.
[4] M. Sugawara, S.-Y. Choi, D. Wood, Ultra-high-definition television (Rec. ITU-R BT. 2020): A generational leap in the evolution of television [standards in a nutshell], IEEE Signal Process. Mag. 31 (2014) 170–174.
[5] P.E. Debevec, J. Malik, Recovering high dynamic range radiance maps from photographs, in: Proc. 24th Annu. Conf. Comput. Graph. Interact. Tech., 1997, pp. 369–378.
[6] A.G. Rempel, M. Trentacoste, H. Seetzen, H.D. Young, W. Heidrich, L. Whitehead, G. Ward, Ldr2hdr: on-the-fly reverse tone mapping of legacy video and photographs, ACM Trans. Graph. 26 (2007) 39.
[7] L. Meylan, S. Daly, S. Süsstrunk, The reproduction of specular highlights on high dynamic range displays, Color Imaging Conf. (2006) 333–338.
[8] Y. Huo, F. Yang, L. Dong, V. Brost, Physiological inverse tone mapping based on retina response, Vis. Comput. 30 (2014) 507–517.
[9] B. Masia, A. Serrano, D. Gutierrez, Dynamic range expansion based on image statistics, Multimed. Tools Appl. 76 (2017) 631–648.
[10] H.-L. Shen, H.-G. Zhang, S.-J. Shao, J.H. Xin, Chromaticity-based separation of reflection components in a single image, Pattern Recognit. 41 (2008) 2461–2469.
[11] K.I. Naka, W.A.H. Rushton, S-potentials from colour units in the retina of fish (Cyprinidae), J. Physiol. 185 (1966) 536–555.
[12] Z. Xie, T.G. Stockham, Toward the unification of three visual laws and two visual models in brightness perception, IEEE Trans. Syst. Man. Cybern. 19 (1989) 379–387.
[13] T. Horiuchi, S. Tominaga, HDR image quality enhancement based on spatially variant retinal response, EURASIP J. Image Video Process. 2010 (2010) 438958.
[14] EMPA Media Technology, < http://empamedia.ethz.ch/hdrdatabase/index.php > (accessed 21 November 2017).
[15] HDR-Eye: Dataset of High Dynamic Range Images with Eye Tracking Data, < https://mmspg.epfl.ch/hdr-eye > (accessed 9 July 2018).
[16] S. Lee, G.H. An, S.-J. Kang, Deep Chain HDRI: Reconstructing a high dynamic range image from a single low dynamic range image, arXiv Prepr. arXiv1801.06277, 2018.
[17] F. Banterle, A. Artusi, K. Debattista, A. Chalmers, Advanced High Dynamic Range Imaging, second ed., AK Peters (CRC Press), New York, 2017.
[18] R. Mantiuk, K.J. Kim, A.G. Rempel, W. Heidrich, HDR-VDP-2: a calibrated visual metric for visibility and quality predictions in all luminance conditions, ACM Trans. Graph. 30 (2011) 40.
[19] T.O. Aydin, R. Mantiuk, K. Myszkowski, H.-P. Seidel, Dynamic range independent image quality assessment, ACM Trans. Graph. 27 (2008) 69.